Numerical Investigation of Flow around Groins in Barotropic Condition

Mojtahedi Alireza, Omdehghiasi Hamed, Lotfollahi-Yaghin Mohammad Ali, and Hokmabady Hamid
Department of Water Resources Engineering, University of Tabriz, Tabriz, Iran
Email: {mojtahedi, lotfollahi}@tabrizu.ac.ir, hamedomdehghiasi@ymail.com, h.hokmabady@gmail.com

***Abstract*—Groins are a kind of structures which constructed to prevent the coastal areas from erosion and to manage the direction of flow. However, the groin body and related flow features are the main causes of local corrosion. In this study, we investigate the flow patterns around refractive and right-angle groins. The flow characteristics around a refractive groin are compared numerically and study to achieve a reliable right-angle groin of various projected lengths. The results indicate that the relation between the thalweg height and geometry of the channel and groin length can be approximated using linear formulas regardless of internal celerity in the flow region.**

***Index Terms*—groyne, barotropic current, baroclinic recirculation area, numerical modelling**

I. Introduction

Seawalls, groins, jetties and other shoreline stabilization structures have had tremendous impacts on our nation's beaches. Shoreline structures are built to alter the effects of ocean waves, currents and sand movement. They are usually built to "protect" buildings that were built on a beach that is losing sand. Groins are dynamic structures that are built to alter the effects of ocean waves and longshore currents. Shore protection structures which extend from the beach backshore into the surf zone, perpendicular to the shoreline. A groin is intended to build up an eroded beach by trapping littoral drift or to retard the erosion of a stretch of beach. Often mis-identified as jetties. Catching and trapping of a part of sediment moving in a surf zone (mainly in a longshore direction), as well as reduction of the sediment amount transported seawards, are the principle functions of the groin. Experiments have shown that when waves are under poor equilibrium conditions, groins disperse the energy of the moving water and drive it onto the adjacent sandy beach. This phenomenon causes sediment accumulation. Larger waves, typically during storms, are responsible for the removal of sediment from the coast and its conveyance out into relatively deep water. Synergistic effects can cause undesirable side effects in coastal area. A coastal area can cause undesirable side effects due to synergistic effects. New methods to increase groin permeability include lowering offshore crest elevations, notching and/or shortening of the groin and increasing material porosity to allow a finite amount of sediment to pass over or through the groin. When incorporated with beach nourishment, permeable groins have proven to be effective in limiting overall project losses and subsequently extending the longevity of beach fills. The performance of groins improves when they are combined with other coastal protection strategies. By detailed coastal investigations, especially during storm periods, a better understanding can be gained of the seasonal changes and their interaction with groins and other coastal structures such as jetties, breakwaters, and seawalls. In particular, we can determine the role they play in scouring at the base of coastal structures and the geotechnical parameters of perpendicular shore sediment transport to the shore. One of the major environmental uses of groins is related to biological functions. Groins protect organisms from natural hazards such as floods. Material exchange processes in the vicinity of groins are crucial for ecological habitats since the developed flow structure and resultant mixing may be advantageous for fish, plankton species, and other marine organisms. Since nutrients can accumulate in the recirculation area, this region is also ideal for juvenile fish [1], [2]. Groins construct in various forms, whereas their flow and sediment patterns are different from each other. This structure could be made in the forms of the combination of right, downward or upward groyne (Fig. 1). According to studies, downward groyne exacerbates erosion around groyne abutment and creates a deeper erosion hole. Since one of the objectives of groyne construction is to establish conditions for the deposition of sediments, therefore, it should be considered in their design process [3]. Downward groynes in comparison to right groynes enhance sedimentation in the groyne field. In this type of groyne, suspended material in the water of the groyne deposited (especially in the upstream) due to the creation of vortexes. Downward groynes are not well suited to protect the banks of river erosion. In these structures, secondary current penetration of groyne field often causes destruction and erosion and in turn is hazardous for the health of the structure. Right groyne also covers fewer protecting area. However, downward groyne comparing to the other types of groynes, is suited to protect the flanks from the risk of erosion and achieving goals of sedimentation and formation of a thick sedimentary layer in the space between the groynes. In addition to the groynes length and direction, their shapes are effective on the performance and outcomes of erosion and sedimentation [3]. In right-angle groins, a wider

Manuscript received October 24, 2015; revised May 4, 2016.

doi: 10.18178/ijscer.5.4.285-291

abutment is used to reduce erosion and prevent the spread of localized erosion holes.

There are three distinct modes of right-angle groin: a flat abutment (usually circular), a T-shaped groin, and an L-shaped groin. Some elementary studies have examined three-dimensional simulation of turbulent flow around the right groyne in the right channel. They have used rectangular grids for meshing the channel and their results are compared with experiments. Also shear stress at the bottom, deposition, and erosion around groyne due to its conduct has been studied [4].

Group groyne can compensate the deleterious effects of a single groyne. In a group groyne, numbers of groynes and the space between them are important factors in flow characteristics, and by increasing the distance of groynes from the criteria value, they don't have an acceptable performance.

The effects of the geometry on the flow region around the groin, including the ratio of length to width in the separation zone, are represented by the numbers and shapes of the vortex. When this ratio tends to one, a vortex is created. If the ratio is higher, there is satisfactory space for the creation of two constant vortices [5]. Turbulent flows around the groins were also simulated numerically and experimentally. Using a third-order interpolation method in a 2D domain, the authors measured the flow celerity and the amount of the vortices by varying the position of the groins [6].

The finite difference method is the subset case of the Finite Volume Method (FVM) that is applied commonly on structures meshing. Therefore, FVM mostly used for natural complex geometry for solving integrating equations [7]. The simulation of large vortices around the groyne was predicted in right paths in some studies. A small-scale model of meshing by combining the Poisson equation were used for the analysis of secondary flow near the groyne and the finite volume method were used for discretization of Navier-Stokes equations [8].

The flow around complex geometries, such as hydrofoils, has also been considered by a number of studies. Because of the difficult geometry of these structures, the authors suggest that an appropriate mesh be applied to achieve greater accuracy [9], [10].

In this study, we investigated the flow characteristics in a channel four meters in length and two meters in width using an image processing technique. In a previous study, groin flow characteristics had been determined for various input velocities, arm lengths, and angles of refraction [11]. We used Kang et al.'s paper to validate our study results with respect to the refractive groin.

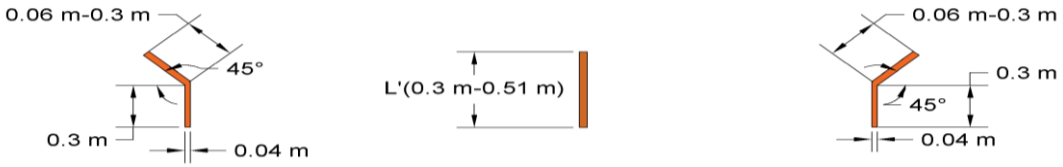

Figure 1. Types of groin; (a) Downstream refractive groin (b) Right-angle groin (c) Upstream refractive groin

II. Methodologies

A. Hydrodynamic Around the Structures

The flow area around the groyne has been divided into the main flow area and the recirculation area that formed in the downstream part of the groyne. The main flow area is the section where the flow is interrupted by the groyne. Thus, as thalweg changes, the flow width, and the flow velocity decreases and increases, respectively. Thalweg refers to the maximum line of flow velocity. The diverse flows in the recirculation area diminish the flow velocity compared to the existing river bed. Thus, it can protect the embankment from erosion, provide ecological space for various types of underwater species, and play the role of a refuge in flood times.

The refractive groyne is a structure with right-angle and arm-length sections (Fig. 2). This kind of the structures can be used to be an arrangement of a right-angle and a downstream or upstream groyne.

Flow change around their body in a manner which depends on the length ratio (*L/B*), in which L and B are the length and width of the channel, respectively, and the dispersion rate of the groin (*p*). In a known category, the groins are classified as permeable or impermeable, based on their construction materials. The impermeable groin is one through which there is no fluid diffusion. The penetration rate is defined as the ratio of the reflected energy to the incident energy of the groin. In this research, we have assumed the groin to be impermeable [12].

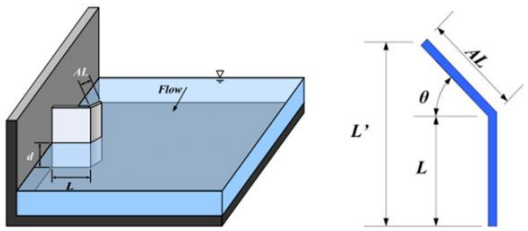

Figure 2. Refractive groin: (a) Location in channel (b) Geometry definition [11]

As also mentioned, the canal length were reduced to 11.5 meters. The output hydrography or surface elevation resulting from the analysis of the main channel along the inner and outer borders of the reduced channel length, were applied as the boundary conditions.

Different cases were modeled with the angles of 45 and 135 degrees and different groin lengths. The results were then compared with those of the reduced channel

model with arm lengths equal to the length of the right-angle body of the groin. Furthermore, the flow region around the projected length of the refractive groin were measured and the observed results compared with the test results to assess the effectiveness of the groin arm.

B. The Governing Equations and Solving Methods

After meshing the computing environment, the equilibrium equations for the shallow waters used for the model analysis. This model is based on a solution for 3D incompressible Reynolds-averaged Navier-Stokes equations, based on the assumptions of Boussinesq approximation and hydrostatic pressure.

The continuity and momentum equations were formulated as shown in Eq. (1) to Eq. (3):

$$\frac{\partial u}{\partial x}+\frac{\partial v}{\partial y}+\frac{\partial w}{\partial z}=S \tag{1}$$

$$\begin{aligned}&\frac{\partial u}{\partial t}+\frac{\partial u^2}{\partial x}+\frac{\partial (vu)}{\partial y}+\frac{\partial (wu)}{\partial z}\\&=fv-g\frac{\partial \eta}{\partial x}-\frac{1}{\rho_0}\frac{\partial P_a}{\partial x}-\frac{g}{\rho_0}\int_z^\eta \frac{\partial \rho}{\partial x}dz\\&-\frac{1}{\rho_0 h}\left(\frac{\partial S_{xx}}{\partial x}+\frac{\partial S_{xy}}{\partial y}\right)+F_u+\frac{\partial}{\partial z}\left(\upsilon_t\frac{\partial u}{\partial z}\right)+u_sS\end{aligned} \tag{2}$$

$$\begin{aligned}&\frac{\partial v}{\partial t}+\frac{\partial v^2}{\partial y}+\frac{\partial (uv)}{\partial x}+\frac{\partial (wv)}{\partial z}\\&=-fu-g\frac{\partial \eta}{\partial y}-\frac{1}{\rho_0}\frac{\partial P_a}{\partial y}-\frac{g}{\rho_0}\int_z^\eta \frac{\partial \rho}{\partial y}dz\\&-\frac{1}{\rho_0 h}\left(\frac{\partial S_{yx}}{\partial x}+\frac{\partial S_{yy}}{\partial y}\right)+F_v+\frac{\partial}{\partial z}\left(\upsilon_t\frac{\partial v}{\partial z}\right)+v_sS\end{aligned} \tag{3}$$

where η is the surface elevation; d is the still water depth; h is the total water depth (h= η + d); u, v, and w are the velocity components in the x, y, and z direction, respectively; f is the Coriolis parameter; S_{ij} is the matrix of the radiation stress tensors; υ_t is the vertical turbulent (or eddy) viscosity; F_u and F_v are horizontal stress terms that are described using a gradient stress relation; P_a is the atmospheric pressure; ρ_0 is the reference density of water. S is the amount of the discharge due to point sources, and u_s and v_s are the speed at which the water is discharged into the ambient water in various directions. The horizontal stress terms are shown in Eqs. (4) and (5), as follows:

$$F_u=\frac{\partial}{\partial x}\left(2A\frac{\partial u}{\partial x}\right)+\frac{\partial}{\partial y}\left(A\left(\frac{\partial u}{\partial y}+\frac{\partial v}{\partial x}\right)\right) \tag{4}$$

$$F_v=\frac{\partial}{\partial x}\left(A\left(\frac{\partial u}{\partial y}+\frac{\partial v}{\partial x}\right)\right)+\frac{\partial}{\partial y}\left(2A\frac{\partial u}{\partial y}\right) \tag{5}$$

where A is the horizontal turbulent viscosity. If the density is baroclinic—a function of salinity and temperature—then other types of equations (transport equations) must be added to the previous equation and these should be solved simultaneously. The spatial discretization of the basic equations is accomplished using a cell-centered finite volume method. The spatial area is discretized by subdividing the continuum into non-overlapping meshes. In the horizontal plane, an unstructured grid is used; however, in the vertical domain in the 3D model, a structured mesh can be used. In the 2D model, the elements can be triangles or quadrilateral elements. In the 3D model, the elements can be prisms or bricks whose horizontal faces are triangles and quadrilateral elements, respectively [13]. For the shallow water equations in Cartesian coordinates, the Courant-Friedrich-Levy (CFL) number is defined in order to control model instability and prevent error distribution. As such, if an error is entered in the numerical analysis, the error in the next steps should not growth. Since two types of equations—hydrodynamic and transport—should be solved, so two CFL numbers must be demarcated. Thus, two types of stability numbers were defined for the hydraulic (CFL_{HD}) and transport (CFL_{AD}) equations. These CFL numbers for the hydrodynamic and transport equations are calculated using Eq. (6) and Eq. (7), as follows:

$$CFL_{HD}=\left(\sqrt{gh}+|u|\right)\frac{\Delta t}{\Delta x}+\left(\sqrt{gh}+|v|\right)\frac{\Delta t}{\Delta y} \tag{6}$$

$$CFL_{AD}=(|u|)\frac{\Delta t}{\Delta x}+(|v|)\frac{\Delta t}{\Delta y} \tag{7}$$

where h is the total water depth, u and v are the speed components in the x and y directions, Δx and Δy are the typical length scale of the elements in the x and y directions and Δt is the time step intervals [14].

C. Turbulence Modeling

Numerical analysis and estimation of the turbulence has been, and to this date still is, the vital problem of fluid dynamics, mainly for the concepts of the computational fluid dynamics. The main struggle arises from the stochastic or chaotic nature of turbulence occurrences. Because of this unpredictability, it has been regular to work with the time averaged forms of the governing equations, which inevitably results in terms involving higher order correlations of fluctuating quantities of flow variables. The semi empirical mathematical models introduced for calculation of these unknown relationships form the source for turbulence modeling [15]. Smagorinsky used the expression of sub-grid scale transport by the correlation of effective eddy viscosity to a characteristic length scale. The sub grid scale eddy viscosity is shown as follows:

$$A=C_S^2.L^2.\sqrt{2S_{ij}.S_{ij}}. \tag{8}$$

where C_S is Smagorinsky constant (the Smagorinsky constant is selected between 0.25 to 1), and L is the characteristic length and strain rate is shown in Eq. (9) [16]:

$$S_{ij}=\frac{1}{2}\left(\frac{\partial u_i}{\partial x_j}+\frac{\partial u_j}{\partial x_i}\right) \tag{9}$$

III. Results

A. Velocity Profile Qualities

Fully developed flow is supposed for the entrance of the channel. Velocity profiles at various distances and at various locations has been shown in Fig. 3 and due to

non-slipping condition of the velocity at the channel wall, velocity is zero along the wall. After encountering the groin, the maximum velocity increased because of constant flow rate and negative velocity. Before the flow encountered the groin, its influence on the thalweg line and the maximum rates location of the currents and vortices has been observed. To identify areas susceptible to erosion and the deposition of sediment, derivation of the flow pattern was required. Identifying the areas susceptible to erosion, illustrating these areas qualitatively was possible based on the flow characteristics. Notice that the order of the terms DRG (URG) xvy denotes a downstream or upstream groin for which x denotes the groin arm length and y is the input speed in centimeters per second, for modes 1 to 5 (Table I).

TABLE I. MODEL CHARACTERISTICS

NO.	Case	L (m)	AL (m)	Θ (degree)	d(m)	$L'(m)$	U_{in} (m/s)
1	URG(DRG)01v25(40)	0.3	0.06	45(135)	0.15	0.34	0.25(0.4)
2	RG01v25(40)	0.34	0	45(135)	0.15	0.34	0.25(0.4)
3	URG(DRG)02v25(40)	0.3	0.12	45(135)	0.15	0.38	0.25(0.4)
4	RG02v25(40)	0.38	0	45(135)	0.15	0.38	0.25(0.4)
5	URG(DRG)03v25(40)	0.3	0.18	45(135)	0.15	0.43	0.25(0.4)
6	RG03v25(40)	0.43	0	45(135)	0.15	0.43	0.25(0.4)
7	URG(DRG)04v25(40)	0.3	0.24	45(135)	0.15	0.47	0.25(0.4)
8	RG04v25(40)	0.47	0	45(135)	0.15	0.47	0.25(0.4)
9	URG(DRG)05v25(40)	0.3	0.3	45(135)	0.15	0.51	0.25(0.4)
10	RG05v25(40)	0.51	0	45(135)	0.15	0.51	0.25(0.4)

The analysis for the right-angle groin is carried out for the five projection lengths of the refractive groin—a total of 10 cases with input velocities of 0.25 m/s and 0.4 m/s. An experimental work was carried out by Kang *et al.* (2011) [11] around a refractive groin, rather than a right-angle groin, and the flow characteristics was gained based on the experimental work. Evaluating flow characteristics by less discrepancy with experiments for a right-angle groin is analyzed in this paper. As a result, some of the flow characteristics of the right-angle groin showed great discrepancy with those from refractive groin by Kang *et al.*(2012) [17]. Therefore, if some of the flow characteristics show acceptable results, similar to those of the experiments, idea of replacing the right-angle groin with a refractive groin by a projected length would be reasonable. As the flow passed the groin, two vortices are created and the intensity of the secondary vortex in the right-angle groin is generally weakened. Moreover, the maximum speed occurred at a significant distance from the groin tip because of the presence of the groin arm. This is resulted in a smaller boundary layer near the groin on the opposite wall. The length of the secondary vortex tended to increase with increasing arm length of the refractive groin. Velocity contours and streamlines for the downstream and upstream refractive groins and the right-angle groin has been shown in Fig. 4 to Fig. 8. Obviously, three vortex centers were created due to the refractive groin, and URG had greater intensity than the DRG groin.

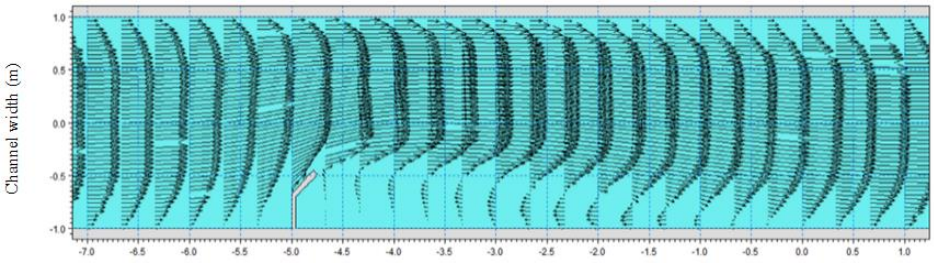

Figure 3. Sketch of velocity profile qualities for the URG groin

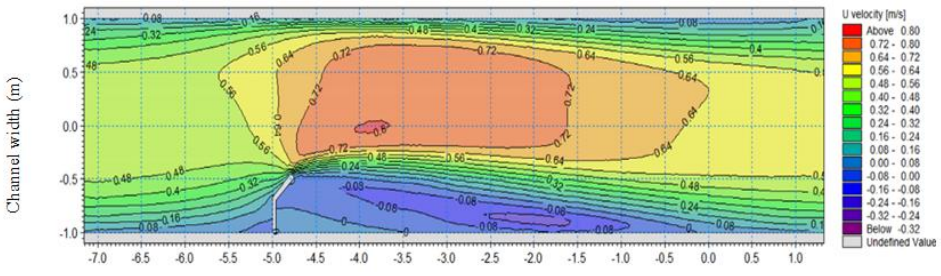

Figure 4. Velocity contour lines of DRG05v40

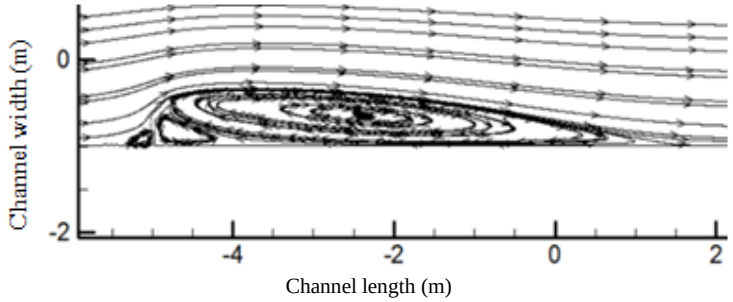

Figure 5. Stream line of DRG05v40

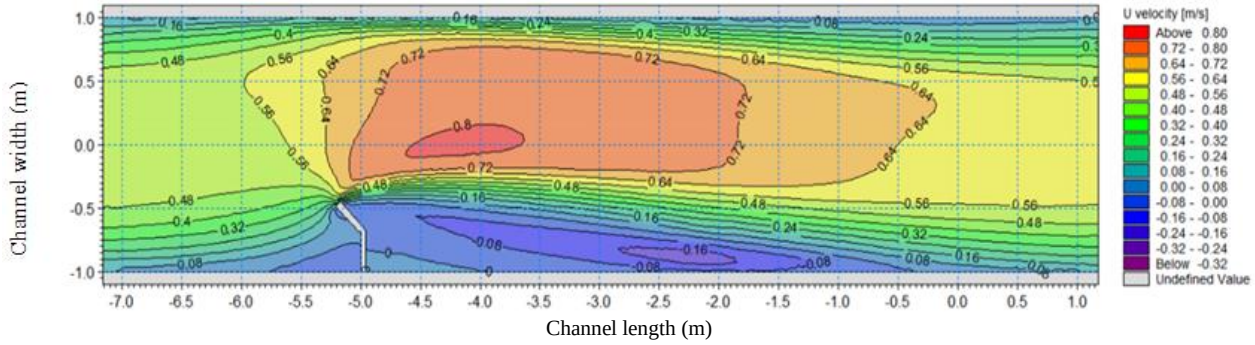

Figure 6. Velocity contour lines of URG05v40

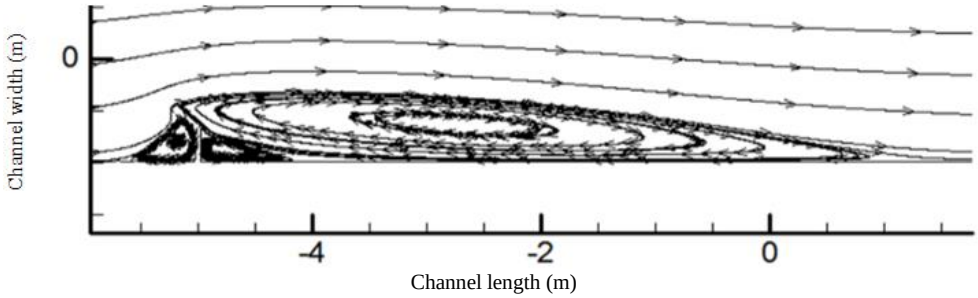

Figure 7. Stream line of URG05v40

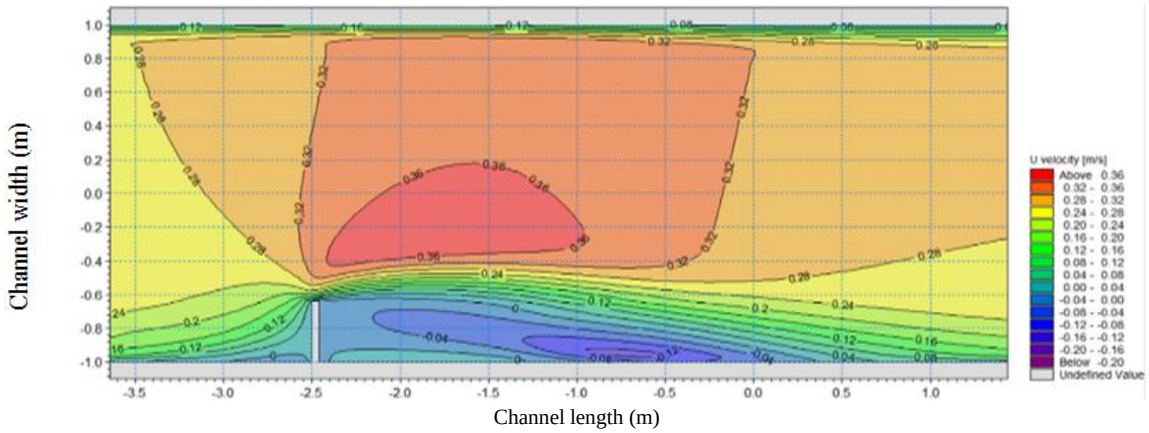

Figure 8. Velocity contour lines of RG01v25

Three vortex centers were created due to groin conduction. These vortices play a major role in the associated erosion and sedimentation processes. Some significant points has been drawn in Figs. 4 to 8. Groin types and shapes have a significant impact on the size and number of vortices. By reducing the groin length for right-angle groins, smaller vortices tend to disappear and afterwards and only one vortex center remains. Type of the downstream or upstream refractive groin has a major role in vortex generation. In the upstream refractive groin, the vortex created after the flow encounters the groin is more critical. In the downstream refractive groin, the vortex that is created prior to encountering the groin, has a more critical value than the secondary vortex that

appears after the groin. Therefore, numbers and sizes of the vortices are one of important indicators of the sediment transport processes.

B. Barotropic Flow Characteristics

In this section, the flow characteristics, including the length and width of the recirculation area, the thalweg height, the maximum velocity and the separation angle of the groin tip with those in the experiments has been compared. In Fig. 9(a) to 9(d), the horizontal axis is the interval error and the vertical axis is the error of the frequency percentage of the desired state. Frequency error refers to the comparison of the analysis results with the experimental results in all cases, and the error range is the discrepancy interval. As an example, in Fig. 9(a), 15.79 percent of the DRG groins' total cases (20 refractive groin analyses) show less than 10% discrepancy in separation length characteristic Results of DRGL and URGL show similar characteristics to right-angle groins. These results are compared with experimental results for downstream and upstream groins, respectively.

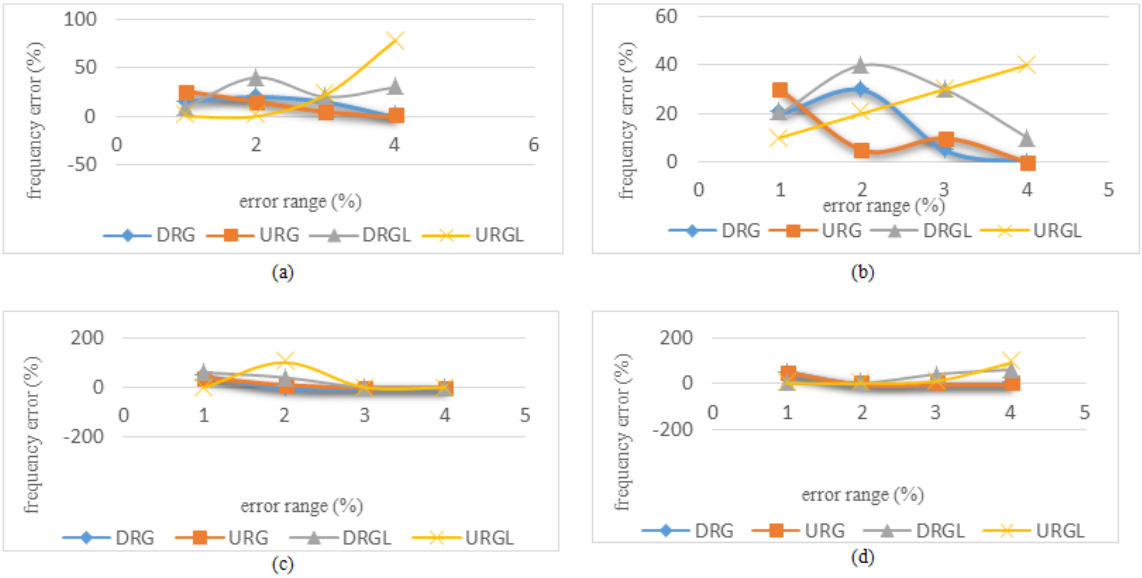

Figure 9. Comparison of flow characteristics with those from experimental work [Kang *et al*. 2011] on barotropic flow: (a) separation length; (b) separation height; (c) maximum velocity; (d) thalweg height

Therefore, the geometry of groins, in both right-angled and refractive groins, has little effects on the maximum speed to the relative average speed. Arm length of the groin in the DRG groin, apart from the angular separation, had less effect than that in the URG groin. As flow characteristics were acquired, dimensionless charts, as a recommendation of the reference case study, are plotted. Each of these diagrams, including the schematic comparisons with the experimental results, have been estimated with a nonlinear equation (Fig. 10). Correlations are not good approximations of the linear equation in some cases, but the relationship between the thalweg height and the aspect ratio of the groin arm length to the projection of groin length is relatively significant. Therefore, regardless of the input rate variation, increasing or decreasing the ratio of the arm length to the projection of the groin, causes the thalweg height to increase and decrease, respectively. Thus, Eq. 10 is used to correlate and estimate this parameter. Eq. (10) is achieved:

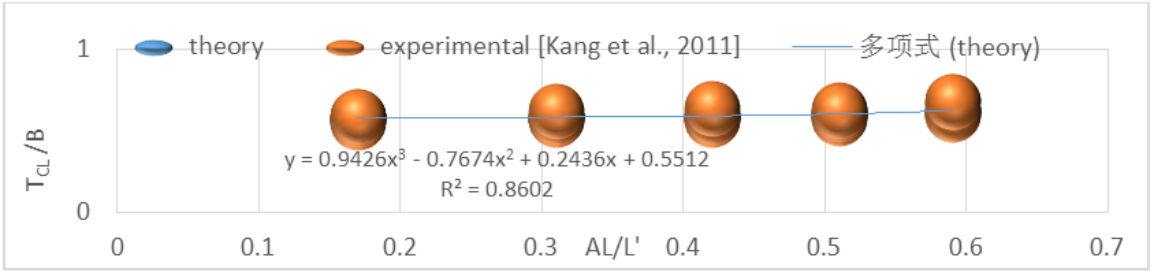

Figure 10. Nonlinear variation of thalweg height rate to arm length rate

$$\frac{T_{CL}}{B} = 0.9426\left(\frac{AL}{L'}\right)^3 - 0.7674\left(\frac{AL}{L'}\right)^2 + 0.2436\left(\frac{AL}{L'}\right) + 0.5512 \quad (10)$$

where T_{CL}, B, AL and L are the thalweg height, channel width, groin arm length, and projected length of groin, respectively.

IV. Conclusion

In this study, the flow field around the refractive and right-angle groins are investigated with respect to barotropic flows. Also, by introducing some dimensionless parameters and then comparing the flow characteristics and geometries of the channel and groin, a significant relationship found in one of the studied cases. The main results can be concluded as follows: The magnitudes of the recirculation region ascent to be larger for increased refractive-groin arm length. The groin body shape, with respect to right-angle or refractive types, had limited effects on the extreme velocity to mean velocity ratio between the flow features. Thalweg height increased with increasing arm length at different input velocities. An extreme increase in the input velocity of 0.4 m/s and 0.25 m/s, yielded 9% and 8% increases in the DRG groin and 8% and 8% increases in the URG groin. The correlation between the thalweg height and the aspect ratio of the arm length identified as being objectively important. Finally, a nonlinear equation were proposed to model the interaction between these parameters.

Nomenclature

URG	Upstream refractive groin
DRG	Downstream refractive groin
RG	Right-angle groin
URGL	Right-angle groin in comparison with URG
DRGL	Right-angle groin in comparison with DRG
L	Groin right-angle Length
AL	Groin arm length
L’	Groin projected length
d	Water depth
Ɵ	Arm angle of refractive groin

References

[1] B. Hentschel and A. Anlauf, “Ecological optimization of groynes in the elbe river,” in *New Insights in the Physical and Ecological Processes in Groyne Fields*, A. van Mazijk and V. Weitbrecht, Eds., Delft, 2002, pp. 121–133.

[2] Z. Marton, T. Tamas, and J. Janos, “Numerical investigation of chaotic advection past a groyne based on laboratory flow experiment,” *Elsevier, Advances in Water Resources*, vol. 71, pp. 81-92, 2014.

[3] W. S. J. Uijttewaal, “Effects of groins layout on the flow in groins fields. Laboratory experiments,” *Journal of Hydraulic Engineering*, vol. 131, no. 9, pp. 782-791, 2005.

[4] S. Ouillon and D. Dartus, “Three-Dimensional computation of flow around groyne,” *Journal of Hydraulic Engineering*, vol. 123, no. 11, pp. 962-970, 1997.

[5] W. S. J. Uijttewaal, D. Lehmann, and A. van Mazijk, “Exchange processes between a river and its groyne fields: Model experiments,” *Journal of Hydraulic Eng*., vol. 127, no. 11, pp. 928–936, 2001.

[6] S. Giri, Y. Shimizu, and B. Surajata, “Laboratory measurement and numerical simulation of flow and turbulence in a meandering-like flume with spurs,” *Flow Measurement and Instrumentation*, vol. 15, pp. 301-309, 2004.

[7] P. A. Sleigh, P. H. Gaskell, M. Berzins, and N. G. Wright, “An unstructured finite volume algorithm for predicting flow in rivers and estuaries,” *Journal of Computer and Fluids*, pp. 479-508, 1997.

[8] X. L. Tang, Z. C. Chen, and F. Yang, “Dynamic large eddy simulation of secondary flow near a groyne,” *International Journal of Nonlinear Sciences and Numerical simulation*, vol. 7, no. 3, pp. 257-262, 2006.

[9] F. Celic, Y. A. Ozden, and S. Bal, “Numerical simulation of the flow around two-dimensional partially cavitating hydrofoils,” *Journal of Marine Science and Application. Springer*, vol. 13, pp. 245-254, 2014.

[10] M. A. Lotfollahi, A. Mojtahedi, M. M. Ettefagh, and M. H. Aminfar, “Experimental investigation of TARMAX model for modeling of hydrodynamic forces on cylinder-like structures,” *Journal of Marine Science and Application*, no. 10, pp. 281-288, 2011.

[11] K. Joongu, Y. Hongkoo, and K. Sungjung, “Experimental study on the flow characteristics around the refraction groyne,” *Scientific Research*, pp. 842-850, 2011.

[12] K. Joongu, Y. Hongkoo, and K. Sungjung, “An experimental study on tip velocity and downstream recirculation zone of single groynes of permeability change,” *Journal of Civil Engineering*, vol. 9, no. 1, pp. 29-38, 2005.

[13] MIKE BY DHI. MIKE 21 & MIKE 3 Flow Model, Hydrodynamic and Transport Module, Scientific Documentation, 2011.

[14] MIKE BY DHI. MIKE 21 & MIKE 3 Flow Model, Softwares’ Help, 2011.

[15] D. C. Wilcox, *Turbulence Modeling for CFD*, DCW Industries, 1994, p. 460.

[16] J. Smagorinsky, “General circulation experiment with the primitive equations,” *Monthly Weather Review*, vol. 91, no. 3, pp. 99-164, 1963.

[17] K. Joongu, Y. Hongkoo, and K. Changsung, “An experimental study on the characteristics of flow around groyne area by install conditions,” *Scientific Research*, pp. 636-645, 2012.